Current Applied Physics 14 (2014) 254–258

Contents lists available at ScienceDirect

Current Applied Physics

journal homepage: www.elsevier.com/locate/cap

Structural, morphological, compositional, and optical properties of single step electrodeposited Cu_2ZnSnS_4 (CZTS) thin films for solar cell application

Seul Gi Lee, Jongmin Kim, Huyn Suk Woo, Yongcheol Jo, A.I. Inamdar, S.M. Pawar, Hyung Sang Kim, Woong Jung, Hyun Sik Im*

Division of Physics and Semiconductor Science, Dongguk University, 3-26 GaPil-Dong, Joong-Gu, Seoul 100-715, Republic of Korea

ARTICLE INFO

Article history:
Received 15 August 2013
Received in revised form
8 November 2013
Accepted 21 November 2013
Available online 1 December 2013

Keywords:
Cu_2ZnSnS_4 (CZTS) thin films
Single step electrodeposition
Rapid thermal annealing
Sulfurization
Solar cell

ABSTRACT

We fabricate a Cu_2ZnSnS_4 (CZTS) absorber layer, by using single step electrodeposition of CZTS precursor, deposited at −1.05 V, followed by high temperature annealing in a sulfur atmosphere. X-ray diffraction pattern indicates that the as-grown sample is amorphous in nature, and polycrystalline CZTS thin films with kesterite crystal structure have been obtained by sulfurization from 450 to 580 °C. Surface morphologies of the as-grown sample show some voids with agglomerated particles. After sulfurization, the morphologies of the annealed samples become more uniform, and dense. EDAX study reveals that the sulfurized samples are nearly stoichiometric, being Cu-rich and S-deficient in composition. The band gaps of the annealed samples are found to be in the range from 1.9 to 1.5 eV.

© 2013 Elsevier B.V. All rights reserved.

1. Introduction

In order to offer an alternative to fossil resources, and reduce the exhaust of green house gas, many research groups have considered the use of renewable energy. Solar cells could one of the solutions in the near future [1,2]. Kesterite Cu_2ZnSnS_4 (CZTS) thin films are attracting a lot of interest as an alternative system to $Cu(In,Ga)Se_2$ (CIGS) thin films, due to their majority carrier type (p-type), proper band gap energy (1.4–1.5 eV), and high optical absorption coefficient ($>10^4$ cm^{-1}) [3]. The most distinguished thing compared with the others, is that they are neither rare metal (In in CIGS) nor toxic materials (Cd in CdTe). The conversion efficiency of sputter-deposited CZTS related solar cell devices has been steadily improved during the last decade [4]. Recently, an efficiency of 11.1% was achieved for a mixed sulfo-selenide device, using a hydrazine-based solution deposition approach [5]. An efficiency of up to 8.4% has been achieved for pure sulfide sputtered CZTS devices [6].

Various groups have tried different methods to fabricate CZTS. They were using vacuum techniques, like pulsed laser deposition [7] sputtering [8–10] and evaporation, and also non-vacuum techniques like electrodeposition [11], spray deposition [12], and chemical bath deposition [13].

In almost all these attempts, the films were annealed to improve structural quality and stoichiometry, which play a key role in solar cell performance. It is reported that CZTS samples having Zn-rich and Cu-poor compositions show better device performance, including higher efficiency, compared with stoichiometric CZTS samples [14]. The improvement in the efficiency of Cu-poor and Zn-rich CZTS solar cells is due to the fact that a Cu-poor composition enhances the formation of Cu vacancies, which gives rise to shallow acceptors in CZTS; while a Zn-rich condition suppresses the substitution of Cu in Zn sites, which results in relatively deep acceptors [15]. With these considerations, it is reasonable to try to develop an electrodeposition method for the fabrication of CZTS absorber films having suitable stoichiometry. Electrodeposition is a promising method for the formation of compound absorber films for photovoltaic applications. On the industrial side, this method makes it possible to obtain large-area CZTS films faster than vacuum processes including sputtering, e-beam evaporation, and pulsed laser deposition. Another advantage is its cost-effectiveness [16–18]. There are two different electrodeposition methods to form CZTS films: (1) a single step electrodeposition that provides all

* Corresponding author.
E-mail address: hyunsik7@dongguk.edu (H.S. Im).

1567-1739/$ – see front matter © 2013 Elsevier B.V. All rights reserved.
http://dx.doi.org/10.1016/j.cap.2013.11.028

constituents from the same electrolyte [19], and (2) sequential electroplating, where to make the final film, different layers are deposited in sequence, followed by annealing in sulfur sources [20].

In this paper, we have analyzed a general reaction mechanism for the formation of an electrodeposited CZTS film, and studied the effect of annealing temperature on the structural, morphological, compositional, and optical properties of the CZTS absorber in a sulfur atmosphere.

2. Experimental

The Cu_2ZnSnS_4 (CZTS) thin films were prepared by using a single step electrodeposition method, from an electrolyte that contains 0.02 M copper sulfate ($CuSO_4$), 0.01 M zinc sulfate ($ZnSO_4$), 0.02 M tin sulfate ($SnSO_4$), and 0.02 M sodium thiosulfate ($Na_2S_2O_3$). 0.2 M tartaric acid and 0.2 M sodium citrate were used as a complexing agent. The electrochemical cell contains a saturated calomel electrode (SCE) as a reference electrode, a graphite electrode as a counter electrode and Mo-coated soda lime glass substrates with a deposition area of 1×5 cm^2 as the working electrode. Before using the Mo-coated glass substrates for electrodeposition, they were cleaned ultrasonically in acetone, methanol, distilled water, and dried under flowing nitrogen. The deposition potential to yield CZTS electrodeposits at room temperature was estimated from cyclic voltammetry using Princeton Applied Research, VERSASTAT3. The uniform and well adhered CZTS thin films were deposited at −1.05 V versus SCE in potentiostatic mode, at room temperature for 45 min. After deposition, the films were rinsed in doubly deionized water. The precursor samples were placed into a graphite box with sulfur powder (50 mg, 99.99%), and the graphite box was then placed in a tubular furnace. We annealed the precursor samples at different annealing temperature from 450 °C to 580 °C for 15 min and we were used for further investigations.

The structural properties of the as-deposited and annealed thin films were studied by using high resolution X-ray diffraction (XRD) with Ni-filtered CuKα radiation (X'pert PRO, Philips, Eindhoven, Netherlands), operated at 40 kV and 100 mA. The surface morphology and compositional study of films were observed by using SEM (model: XL30, FEI, Netherlands) attached with an energy-dispersive X-ray analysis (EDAX) analyzer to measure the sample composition. The optical properties of the films were measured in the wavelength range 350–800 nm by UV–vis-NIR spectrophotometer (Cary 100, Varian, Mulgrave, Australia).

3. Results and discussion

Fig. 1(a) shows a cyclic voltammetry (CV) in the electrolyte containing a mixture of Cu, Zn, Sn, S precursor solutions and Na_3-citrate; and Fig. 1(b) presents a schematic of the electrodeposition for the formation of CZTS film, with a kesterite crystal structure [21]. The pH of precursor solution is adjusted to be 4.5–6, using tartaric acid. In the case of single step electrodeposition, to deposit films at one potential, we have to add complexing agent, to narrow the potential gap [22]. The citrate anion and metal cation form a complex compound, and provide evidence for the reducing metal cation activity in the solution. Also, the citrate can increase the hydrogen evolution overpotential, by shifting the H^+ reduction peak in the negative direction [23]. The wave of current density steadily rises up to −1.05 V, and then decreases, displaying all redox reactions in the tri-sodium citrate and tartaric acid mixed electrolytic bath solution. The general reaction mechanism for electrodeposition of CZTS film is given as [24]:

$$CuSO_4 \rightarrow Cu^{2+} + SO_3^- \quad (1)$$

$$ZnSO_4 \rightarrow Zn^{2+} + SO_3^- \quad (2)$$

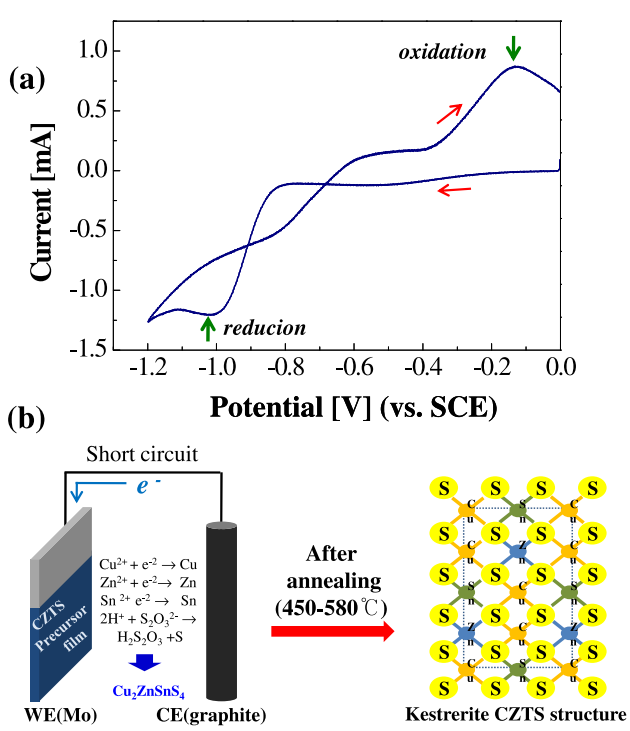

Fig. 1. (a) Cyclic voltammogram of the electrolyte containing Cu, Zn, Sn and S at a scan rate of 10 mV s^{-1}, and (b) Schematic of electrodeposition for CZTS film and kesterite CZTS structure.

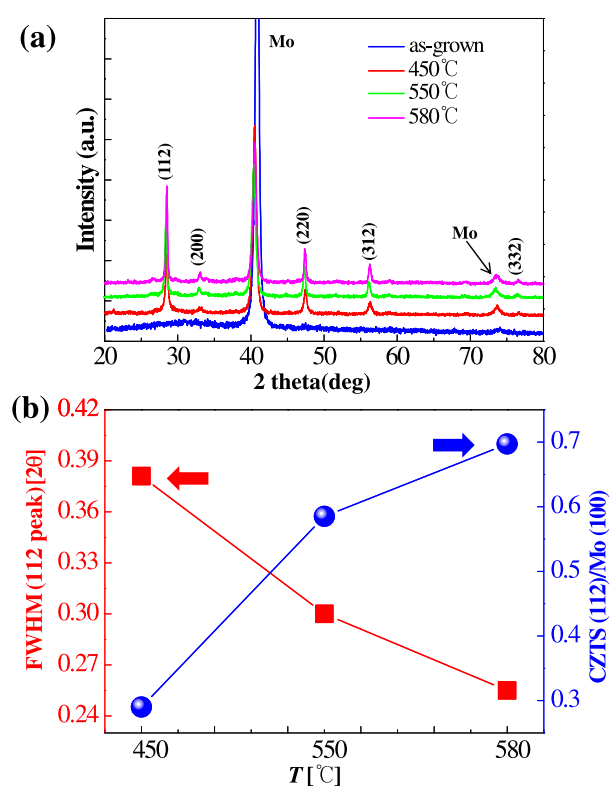

Fig. 2. X-ray diffraction patterns of (a) as-grown and sulfurized CZTS films at 450 °C, 550 °C, and 580 °C, and (b) FWHM of (112) peak of annealed sample.

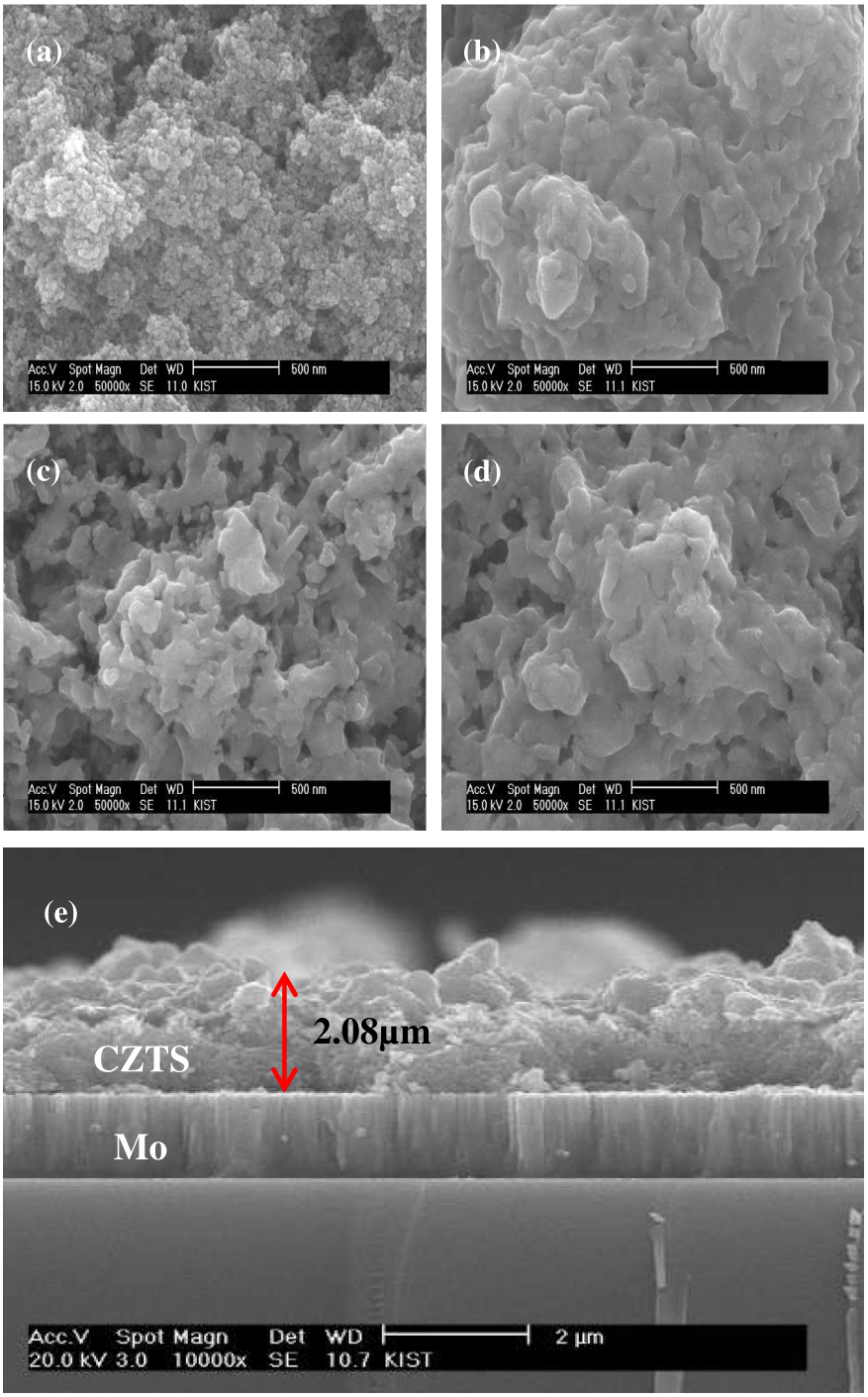

Fig. 3. Plan-view SEM images of (a) as-grown and annealed Cu_2ZnSnS_4(CZTS), with different annealing temperatures of (b) 450 °C, (c)550 °C, and (d)580 °C. (e) Cross-sectional SEM image at 580 °C.

$$SnSO^4 \rightarrow Sn^{2+} + SO_3^- \quad (3)$$

$$Na_2S_2O_3 \rightarrow 2Na^+ + S_2O_3^{2-} \quad (4)$$

$$Cu^{2+} + Zn^{2+} + S^{2+} + 4S_2O_3^{2-} + 14\,e^- \rightarrow Cu_2ZnSnS_4 + 4SO_3^{2-} \quad (5)$$

Through these mechanisms, we can obtain CZTS precursors, and CZTS kesterite structure is formed after the sulfurization process.

Fig. 2(a) is X-ray diffraction of as-grown and annealed CZTS absorber, at 450–580 °C for 15 min, in sulfur atmosphere. The as-grown film is revealed to be amorphous in nature, and the as-grown film is sulfurized at 450 °C in sulfur atmosphere. The major diffraction peaks of the film correspond to (112), (200), (220), (312), and (332) peaks [JCPDS card: 26-0575]. With increase in annealing temperature from 450 to 580 °C, the intensity of the kesterite (112) peak becomes more intense and sharp, due to increasing crystallinity. These results are in agreement with earlier reports [25,26]. Fig. 2(b) shows the FWHM of the (112) peak and the intensity ratio of the CZTS (112)/Mo (100) peak. Also, we calculate

the grain size of the annealed sample, using the following Scherrer formula [27],

$$D = \frac{0.9\lambda}{\beta \cos\theta} \tag{6}$$

where, λ is the X-ray wavelength (0.15406 nm), and β is the FWHM of the film diffraction peak at 2θ, where θ is the Bragg's diffraction angle. The table shows that, as the sulfurization temperature increases from 450 °C to 580 °C, the FWHM decreases from 0.38 to 0.25, hence increases the grain size from 21 nm to 32 nm.

Fig. 3 shows plan-view SEM images of the as-deposited and annealed CZTS thin films. From the figure, it is observed that the precursor film shows non-uniform distribution of agglomerated particles. The annealed CZTS film is shown to be more compact than the as-grown samples, with some voids on the surface. The compositional analysis of as-grown and annealed CZTS sample is shown in Fig. 4. The as-grown sample has less quantity of sulfur. However, after annealing in sulfur atmosphere, it is nearly stoichiometric, with sulfur deficient in composition. Also the quantity of sulfur in sulfurized films decreases with increasing annealed temperature. This may be due to loss of sulfur during the annealing process.

Table 1 shows that the Cu/(Zn + Sn) ratio of as-grown and annealed samples are 1.52, 1.09, 1.01, and 1.13 respectively. All the samples show Cu-rich in composition. Study of the thermodynamic stability of CZTS quaternary compound reveals that the stable chemical potential region for the formation of stoichiometric compound is small. Under these conditions, the dominant defect will be p-type CuZn antisite, which has an acceptor level deeper than the Cu vacancy. For the high performance of CZTS solar cell device, we have to minimize these defects [15]. Thus, with further investigation, we will optimize these conditions, to reduce the quantity of copper.

We measured the absorption and reflectance of sulfurized CZTS films, using a UV–vis-NIR spectrophotometer for optical measurement. Fig. 5 shows the plot of $(\alpha h\nu)^2$ versus photon energy $(h\nu)$ of the annealed CZTS samples. Using the absorption data from the reflectance spectra the energy band gap can be calculated [28,29]:

$$\alpha = A(h\nu - E_g)^{1/2} \tag{7}$$

where α is the absorption coefficient, A is a constant, E_g is the energy gap, and $h\nu$ is the incident photon energy for the annealed CZTS samples. Extrapolation of these curves to zero absorption coefficients ($\alpha = 0$) gave the optical energy. The direct band gap energies decrease from 1.9 to 1.5 eV, with increasing annealing temperature. This decrement in the band gap energies may be due to an increase in the grain size, and a reduction in the grain boundaries with increasing annealing temperature [10]. These results are consistent with our XRD results (Table 2). The band gap energies of 550 and 580 °C annealed samples are in good agreement with the earlier reported E_g value [30,31].

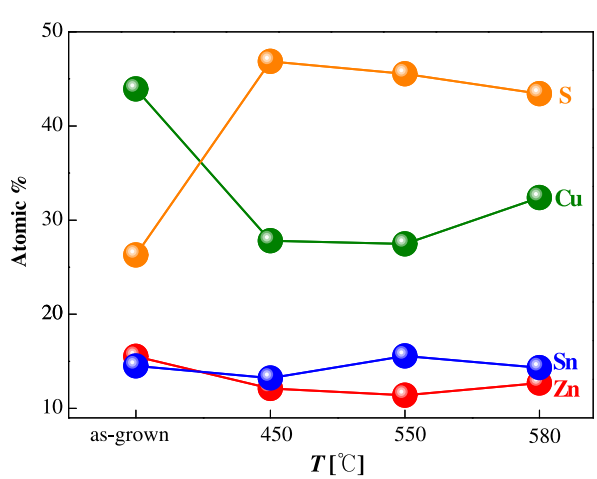

Fig. 4. Atomic composition of as-grown and sulfurized CZTS samples at 450 °C, 550 °C, and 580 °C.

Table 1
The Cu/(Zn + Sn), Zn/Sn, and S/Metal composition ratios of annealed CZTS samples.

	Cu/(Zn + Sn)	Zn/Sn	S/metal
As-grown	1.52	1.06	0.35
450 °C	1.09	0.916	0.84
550 °C	1.01	0.731	0.836
580 °C	1.13	0.952	0.76

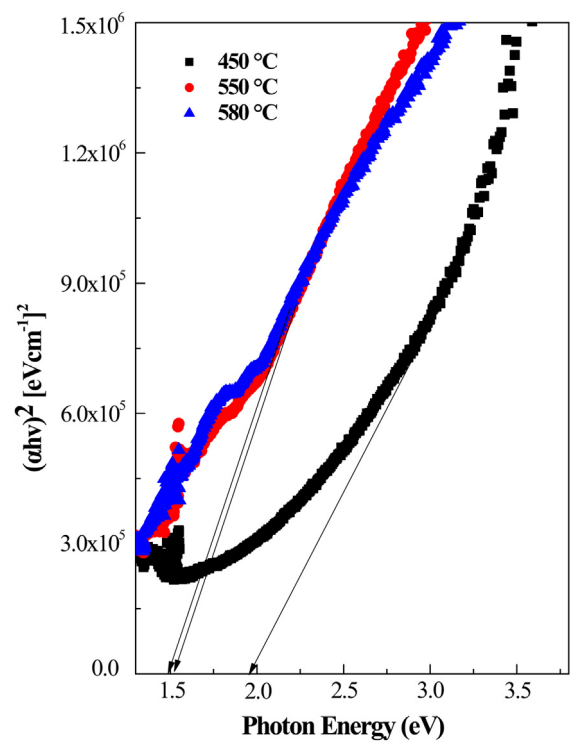

Fig. 5. $(\alpha h\nu)^2$ versus photon energy $(h\nu)$ plot of the annealed CZTS samples.

4. Conclusion

In conclusion, we have fabricated CZTS absorber using single step electrodeposition, followed by high temperature annealing in sulfur atmosphere. The as-grown sample is amorphous in nature, but polycrystalline CZTS thin film with kesterite structure has been obtained, after the annealing process. With increased annealing temperature from 450 °C to 580 °C, the intensity of the kesterite (112) peak becomes more intense and sharp. SEM study shows that

Table 2
Grain size values of the sulfurized CZTS films at 450 °C, 550 °C, and 580 °C.

Annealing temperature (°C)	FWHM (2θ)	Grain size (nm)
450	0.381	21
550	0.3	27
580	0.255	32

the as-grown sample has a non-uniform distribution of agglomerated particles. On increasing the annealing temperature, the films become more uniform and dense. EDAX study reveals that the sulfurized samples are nearly stoichiometric, being Cu-rich and sulfur deficient. The sample that has Cu-rich composition will be formed with some defect, like p-type CuZn antisite. Thus, with further investigation, we will optimize the compositional condition. Optical measurement shows that the direct band gap energies of the annealed CZTS films are found to decrease from 1.9 eV to 1.5 eV. Absorption measurement and band gap energy determination of the CZTS film confirm its applicability to solar cells.

Acknowledgment

This work was partially supported by the National Research Foundation (NRF) of Korea grant funded by the Ministry of Education (Grant Nos. 2012R1A1A2008517 and 2012-00109).

References

[1] K. Jimbo, R. Kimura, T. Kamimura, S. Yamada, W.S. Maw, H. Araki, K. Oishi, H. Katagiri, Thin Solid Films 515 (2007) 5997–5999.
[2] H. Katagiri, K. Saitoh, T. Washio, H. Shinohara, T. Kurumadani, S. Miyajima, Sol. Energy Mater. Sol. Cells 65 (2001) 141–148.
[3] H. Katagiri, K. Jimbo, W.S. Maw, K. Oishi, M. Yamazaki, H. Araki, A. Takeuchi, Thin Solid Films 517 (2009) 2455–2460.
[4] M. Friedlmeier, N. Wieser, T. Walter, H. Dittrich, H.W. Schock, in: Proceedings of the 14th European PVSEC and Exhibition, 1997, p. 10.
[5] T.K. Todorov, J. Tang, S. Bag, Oki Gunawan, Tayfun Gokmen, Yu Zhu, David B. Mitzi, Adv. Energy Mater. 3 (2013) 34–38.
[6] B. Shin, O. Gunawan, Y. Zhu, N.A. Bojarczuk, S.J. Chey, S. Guha, Prog. Photovolt.: Res. Appl. 21 (2013) 72–76.
[7] K. Moriya, K. Tanaka, H. Uchiki, Jpn. J. Appl. Phys. 46 (2007) 5780–5781.
[8] J.S. Seol, S.Y. Lee, J.C. Lee, H.D. Nam, K.H. Kim, Sol. Energy Mater. Sol. Cells 75 (2003) 155–162.
[9] A.I. Inamdar, K.Y. Jeon, H.S. Woo, W. Jung, H.S. Im, J. Korean Phys. Soc. 60 (2012) 1730–1734.
[10] A.I. Inamdar, S.G. Lee, K.Y. Jeon, C.H. Lee, S.M. Pawar, R.S. Kalubarme, C.J. Park, H.S. Im, W. Jung, H.S. Kim, Solar Energy 91 (2013) 196–203.
[11] J.J. Scragg, P.J. Dale, L.M. Peter, Electrochem. Commun. 10 (2008) 639–642.
[12] N. Kamoun, H. Bouzouita, B. Rezig, Thin Solid Films 515 (2007) 5949–5952.
[13] N.M. Shinde, C.D. Lokhande, J.H. Kim, J.H. Moon, J. Photochem. Photobiol. A Chem. 235 (2012) 14–20.
[14] S. Chen, A. Walsh, X.G. Gong, S.H. Wei, Adv. Mater. 25 (2013) 1522–1539.
[15] S. Chen, X.G. Gong, A. Walsh, S.H. Wei, Appl. Phys. Lett. 96 (2009) 021902-1–021902-13.
[16] S.M. Pawar, B.S. Pawar, A.V. Moholkar, D.S. Choi, J.H. Yun, J.H. Moon, S.S. Kolekar, J.H. Kim, Electrochim. Acta 55 (2010) 4057–4061.
[17] W. Septina, S. Ikeda, A. Kyoraiseki, T. Harada, M. Matsumura, Electrochim. Acta 88 (2013) 436–442.
[18] L. Rovelli, S.D. Tilley, K. Sivula, ACS Appl. Mater. Interfaces 5 (2013) 8018–8024.
[19] S.M. Pawar, B.S. Pawar, K.V. Gurav, D.W. Bae, S.H. Kwon, S.S. Kolekar, J.H. Kim, Jpn. J. Appl. Phys. 51 (2012), 10NC27-1–10NC27-4.
[20] L. Guo, Y. Zhu, O. Gunawan, T. Gokmen, V.R. Deline, S. Ahmed, L.T. Romankiw, H. Deligianni, Prog. Photovolt: Res. Appl. (2012) 2332.
[21] D.B. Mitzi, O. Gunawan, T.K. Todorov, K. Wang, S. Guha, Sol. Energy Mater. Sol. Cells 95 (2011) 1421–1436.
[22] F. Chraibi, M. Fahoume, A. Ennaoui, J.L. Delplancke, Phys. Stat. Sol. 186 (2001) 373–381.
[23] Y. Lai, F. Liu, Z. Zhang, J. Liu, Y. Li, S. Kuang, J. Li, Y. Liu, Electrochim. Acta 54 (2009) 3004–3010.
[24] J. Iljina, R. Zhang, M. Ganchev, T. Raadik, O. Volobujeva, M. Altosaar, R. Traksmaa, E. Mellikov, Thin Solid Films 537 (2013) 85–89.
[25] S.W. Shin, S.M. Pawar, C.Y. Park, J.H. Yun, J.H. Moon, J.H. Kim, J.Y. Lee, Sol. Energy Mater. Sol. Cells 95 (2011) 3202–3206.
[26] J.J. Scragg, P.J. Dale, L.M. Peter, Thin Solid Films 517 (2009) 2481–2484.
[27] B.D. Cullity, S.R. Stock, R. Stuart, Elements of X-ray Diffraction, third ed., Prentice Hall, Upper Saddle River, NJ, 2001.
[28] M. Snure, A. Tiwari, Appl. Phys. Lett. 91 (2007) 092123.
[29] J.J. Scragg, P.J. Dale, L.M. Peter, G. Zoppi, I. Forbes, Phys. Stat. Sol. B 245 (2008) 1772–1778.
[30] S. Ahmed, K.B. Reuter, O. Gunawan, L. Guo, L.T. Romankiw, H. Deligianni, Adv. Energy Mater. 2 (2012) 253–259.
[31] J. Paier, R. Asahi, A. Nagoya, G. Kresse, Phys. Rev. B 79 (2009) 115126-1–115126-8.